ChemPubSoc Europe

DOI: 10.1002/chem.201603591

CHEMISTRY A European Journal Full Paper

Chromophores | *Hot Paper*

Physicochemical and Electronic Properties of Cationic [6]Helicenes: from Chemical and Electrochemical Stabilities to Far-Red (Polarized) Luminescence

Johann Bosson,[a] Geraldine M. Labrador,[a] Simon Pascal,[a] François-Alexandre Miannay,[b] Oleksandr Yushchenko,[b] Haidong Li,[c] Laurent Bouffier,[c] Neso Sojic,[c] Roberto C. Tovar,[d] Gilles Muller,[d] Denis Jacquemin,[e] Adèle D. Laurent,[e] Boris Le Guennic,[f] Eric Vauthey,*[b] and Jérôme Lacour*[a]

Abstract: The physicochemical properties of cationic dioxa (**1**), azaoxa (**2**), and diaza (**3**) [6]helicenes demonstrate a much higher chemical stability of the diaza adduct **3** (pK_{R+} = 20.4, $E^{red}_{1/2}$ = −0.72 V) compared to its azaoxa **2** (pK_{R+} = 15.2, $E^{red}_{1/2}$ = −0.45 V) and dioxa **1** (pK_{R+} = 8.8, $E^{red}_{1/2}$ = −0.12 V) analogues. The fluorescence of these cationic chromophores is established, and ranges from the orange to the far-red regions. From **1** to **3**, a bathochromic shift of the lowest energy transitions (up to 614 nm in acetonitrile) and an enhancement of the fluorescence quantum yields and lifetimes (up to 31% and 9.8 ns, respectively, at 658 nm) are observed. The triplet quantum yields and circularly polarized luminescence are also reported. Finally, fine tuning of the optical properties of the diaza [6]helicene core is achieved through selective and orthogonal post-functionalization reactions (12 examples, compounds **4**–**15**). The electronic absorption is modulated from the orange to the far-red spectral range (560–731 nm), and fluorescence is observed from 591 to 755 nm with enhanced quantum efficiency up to 70% (619 nm). The influence of the peripheral auxochrome substituents is rationalized by first-principles calculations.

Introduction

Previously, cationic dioxa, azaoxa, and diaza [6]helicenes (**1**–**3**) have been reported (Figure 1, W,X,Y,Z = H).[1,2] Their preparation involves five straightforward steps to reach a common late-stage intermediate, and then divergent procedures to afford the final products.[3] Compounds **1**–**3** are effective chromophores and can be isolated as single enantiomers (*M* or *P* configurations). Pronounced chiroptical properties have been obtained, for example, electronic circular dichroism (ECD) in both UV and visible spectral windows.[4] Furthermore, regioselective post-functionalization of diaza [6]helicene **3** is possible with both electrophilic and nucleophilic reagents, enabling the introduction of auxochromes in either the 8 and 10 positions or 5 and 13 positions, respectively (helicenes **4** to **15**, see Figures 1 and 7).

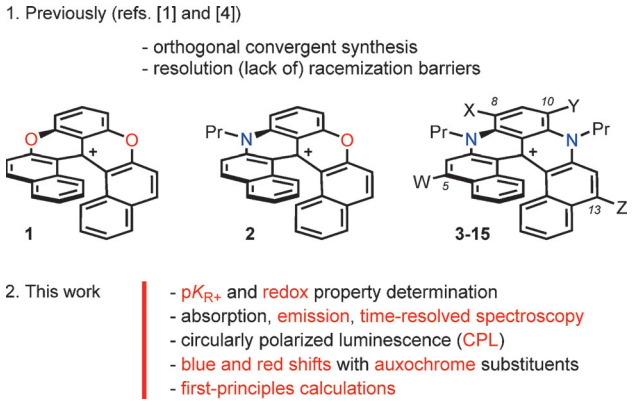

Figure 1. Cationic [6]helicenes (only *P* enantiomers shown): dioxa **1**, azaoxa **2**, and diaza **3**–**15** (W,X,Y,Z = H, halogens, NO_2, CN, aryl, or amines; see Figure 7 for details).

[a] *Dr. J. Bosson, G. M. Labrador, Dr. S. Pascal, Prof. J. Lacour*
Department of Organic Chemistry, University of Geneva
Quai Ernest Ansermet, 30.1211 Geneva 4 (Switzerland)
E-mail: jerome.lacour@unige.ch

[b] *Dr. F.-A. Miannay, O. Yushchenko, Prof. E. Vauthey*
Department of Physical Chemistry, University of Geneva
Quai Ernest Ansermet, 30.1211 Geneva 4 (Switzerland)
E-mail: eric.vauthey@unige.ch

[c] *H. Li, Dr. L. Bouffier, Prof. N. Sojic*
ISM, UMR 5255, University of Bordeaux and CNRS, 33400 Talence (France)

[d] *R. C. Tovar, Prof. G. Muller*
Department of Chemistry, San José State University
1 Washington Square, San José, CA 95192-0101 (USA)

[e] *Prof. D. Jacquemin, Dr. A. D. Laurent*
CEISAM, UMR CNRS 6230, Faculté des Sciences et des Techniques
Université de Nantes, 2, rue de la Houssinière 44322 Nantes (France)
Institut Universitaire de France, 1, rue Descartes
75005 Paris Cedex 05 (France)

[f] *Dr. B. Le Guennic*
Sciences Chimiques de Rennes UMR 6226, CNRS - Université de Rennes 1
Campus de Beaulieu, 35042 Rennes (France)

Supporting information and ORCID number(s) for the author(s) of this article are available under http://dx.doi.org/10.1002/chem.201603591.

Herein, the core properties of cationic helicenes **1** to **3** are reported. Remarkable chemical stabilities are evidenced by measurements of highly positive pK_{R+} values (up to +20.4) and low one-electron reduction potentials. In-depth studies also demonstrate low-energy emissions for **1**–**3** accompanied by large fluorescence quantum yields and lifetimes at wavelengths that are unusual for purely organic helicenes (e.g., **3** at 658 nm: $\phi_{fl}=31\%$ and $\tau=9.8$ ns in acetonitrile).[5] Transient absorption measurements of **1**–**3** indicate that fluorescence and internal conversion are the main decay processes of the lowest singlet excited state. However, upon substitution with a heavy atom such as iodine, intersystem crossing to the triplet state becomes dominant. Circularly polarized luminescence (CPL) of enantiopure samples of **1**–**3** is also reported at low energies (e.g., **2** at ≈614 nm: g_{lum} values of −0.0021/+0.0020). Finally and importantly, with modified helicenes **4**–**15**, both absorption and emission properties can be adjusted by the nature of the substituents introduced at the periphery of the helical core. A maximum fluorescence quantum yield of 70% is obtained for **14** (619 nm, W=NHPr; X,Y,Z=H), and the lowest-energy emission is observed for **13** (731 nm, ϕ_{fl} 1%, W,Z=CN; X,Y=H). The influence of the different substitution patterns on the electronic properties is further rationalized by in silico modeling.

Results and Discussion

Core structures (1–3)

Derivatives **1**–**3** are [6]helicenes and triaryl methyl carbenium moieties at the same time.[6] In principle, they can react with nucleophiles in S_N1-like addition processes. Their existence as cations was consequently debatable under neutral and/or basic or reductive conditions. Therefore, pK_{R+} values and one-electron reduction potentials were measured to establish their chemical stability.

Carbenium stability

As electrophiles, triaryl methyl carbenium ions are in fact expected to react with water and form carbinol derivatives after proton loss [Eq. (1)]. This reaction and the corresponding equilibrium constant can be used to characterize the chemical stability of carbocationic structures [Eq. (2)]. For instance, highly stable carbenium ions present a low reactivity, and hence, highly positive pK_{R+} values [Eq. (3)].[2k]

$$R^+ + H_2O \rightleftharpoons ROH + H^+ \quad (1)$$

$$pK_{R+} = C_- + \log\frac{[R^+]}{[ROH]} \quad (2)$$

$$pK_{R+} = C_- + \log\frac{Abs}{1-Abs} \quad (3)$$

Experimentally, the equilibrium can be monitored by UV/Vis absorption spectroscopy, as cationic compounds **1**–**3** are colorful dyes and the corresponding carbinols essentially colorless [Eq. (3)].[1,4] In the case of the most reactive **1**, measurements were performed in 0.1 M sodium borate buffered aqueous solutions using NaOH as base (see Supporting Information).[7] However, with **2** and **3**, equimolar concentrations of carbenium and carbinol species, $[R^+]=[ROH]$, were never reached in aqueous solutions, even at pH 14. For these dyes, the measurements were therefore performed in mixtures of DMSO/water/$Me_4N^+OH^-$, for which the DMSO/water ratio modulates the basicity beyond pH 14.[8] For the calculations, it was then necessary to use the C_- acidity function defined by Laursen and co-workers instead of the regular pH scale.[9] For each carbenium ion, the value of $\log([ROH]/[R^+])$ is plotted versus C_- (Figure 2 and Supporting Information for details). The intercepts with the origin

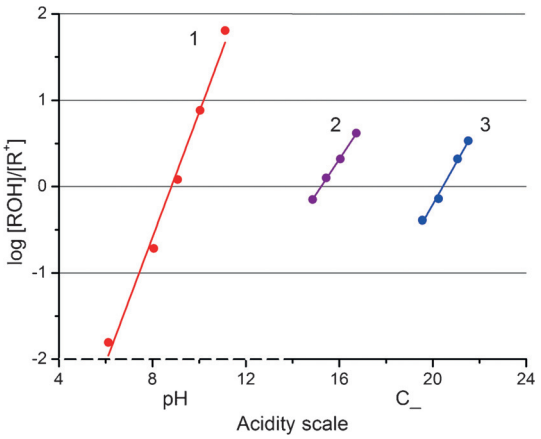

Figure 2. Plots of $\log([ROH]/[R^+])$ versus acidity for dioxa **1** (red), azaoxa **2** (purple), and diaza[6]helicene **3** (blue).

of the linear fitted lines indicate the points at which equimolar concentrations of $[R^+]$ and [ROH] are obtained, and hence, the pK_{R+} values.[10] Finally, values of 8.8, 15.2, and 20.4 were determined for **1**, **2**, and **3**, respectively.[11] As expected, compound **1** is clearly the most electrophilic. Replacement of the oxygen atoms at bridge positions by more electron-donating nitrogen leads to a substantial increase in chemical stability for carbenium ions **2** and **3**. An analogous trend has been observed previously for cationic [4]helicenes[8,12] as well as for related structures.[2k]

Electrochemical properties

For further assessment of the stability of the cationic species, the redox properties of compounds **1**–**3** were characterized. The electrochemical behavior of these species was analyzed by cyclic voltammetry (CV). The CV curves presented in Figure 3 were recorded in degassed acetonitrile solutions containing 1 mM of each of the [6]helicenes and *n*-tetrabutylammonium hexafluorophosphate ($TBAPF_6$) as the supporting electrolyte (data are gathered in Table 1).[13] Diaza [6]helicene **3** exhibits a relatively simple redox behavior (Figure 3). This compound is typically reduced at $E^{red}_{1/2}=-0.72$ V versus Fc/Fc^+, with a peak-to-peak separation (ΔE_{peaks}) of approximately 57 mV evidencing

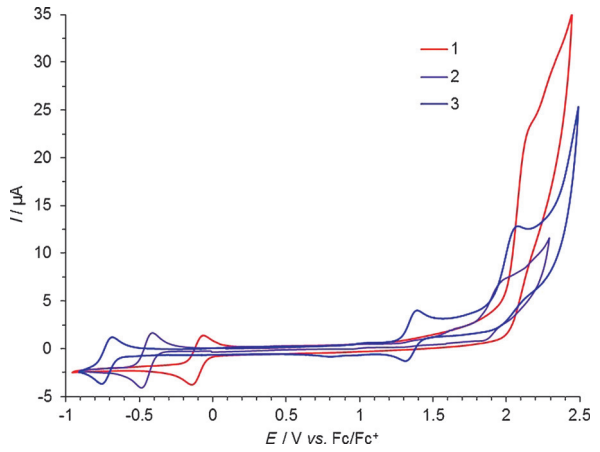

Figure 3. Cyclic voltammograms of 1 mM dioxa (**1**, red), azaoxa (**2**, purple) and diaza (**3**, blue) [6]helicenes, recorded in degassed CH_3CN solution containing 0.1 M $TBAPF_6$ as supporting electrolyte ($\nu = 0.1\ V\,s^{-1}$). The potential was scanned first toward positive values and then toward negative ones.

Table 1. Anodic and cathodic halfwave potentials ($E_{1/2}$) values measured by CV for **1**–**3** in acetonitrile (0.1 M $TBAPF_6$) at a Pt electrode ($\nu = 0.1\ V\,s^{-1}$), E versus Fc/Fc^+. Fundamental gaps and optical gaps for **1**–**3**.

Cpd	$E^{red}_{1/2}$ [V]	$E^{ox1}_{1/2}$ [V]	Fund. gap [eV][b]	Opt. gap [eV][c]
1	−0.12	2.14[a]	2.26	2.15
2	−0.45	1.93[a]	2.38	2.11
3	−0.72	1.40	2.12	1.95

[a] The anodic process is partially irreversible for **2** and fully irreversible for **1**, and therefore, the reported value corresponds to the oxidation peak potential E^{ox}_p for these compounds. [b] Fundamental (Fund.) gap = $E^{ox1}_{1/2} - E^{red}_{1/2}$. For the compounds characterized by irreversible oxidation, the value of $E^{ox1}_{1/2}$ is replaced by the peak potential E^{ox}_p in a first approximation. [c] Optical (Opt.) gap = 0–0 energy.

a reversible monoelectronic transfer generating a neutral species from the cation. The first oxidation also shows a reversible behavior with $E^{ox}_{1/2} = 1.40$ V versus Fc/Fc^+ and $\Delta E_{peaks} \approx 62$ mV. The peak-to-peak separation deviates slightly from ideal, but still points to a reversible one-electron mechanism. The scan rate was varied in the range 0.1–1 $V\,s^{-1}$; the study of the current peak shows a linear evolution with respect to the square root of scan rate (data not shown), which is perfectly consistent with a diffusion-controlled process. A second oxidation is observed at a more anodic potential of around 2 V, and the irreversibility of this process can be assigned to an irreversible oxidative decomposition of the [6]helicene core, which was not investigated further.

With azaoxa **2**, the reductive behavior is apparently unchanged with a single reversible one-electron reduction, albeit occurring at a much less cathodic potential ($E^{red}_{1/2} = -0.45$ V vs. Fc/Fc^+ and $\Delta E_{peaks} \approx 58$ mV). On the other hand, a partially irreversible oxidation process is observed, occurring at large anodic overpotentials ($E^{ox}_p = 1.93$ V vs. Fc/Fc^+). Finally, the electrochemical characterization of dioxa [6]helicene **1** reveals an even easier reduction process ($E^{red}_{1/2} = -0.12$ V vs. Fc/Fc^+ with $\Delta E_{peaks} \approx 60$ mV) but also a very large $E^{ox}_{1/2}$ value (2.14 V vs. Fc/Fc^+) for the fully irreversible oxidation. No improvement of reversibility was observed upon increasing the scan rate (data not shown). This indicates that the replacement of nitrogen atoms by oxygen atoms irreversibly perturbs the oxidation pathways, as the "substitution" clearly destabilizes the corresponding dicationic structures. Notably, a similar structure–activity relationship was observed previously for cationic triangulene dyes.[14] Not surprisingly, the reduction behavior of **2** stands between those of compounds **1** and **3** as a one-to-one comparison reveals cathodic shifts of 0.33 and 0.27 V, respectively. As evidenced through the measurement of the pK_{R+} values of compounds **1**–**3** (vide supra) or observed in the case of other cationic helicenes, the introduction of amino groups in place of the O atoms in the core structures clearly stabilizes the carbocations[2k,12b,d] Overall, the CV investigation reveals a reversible monoelectronic reduction for all three cationic [6]helicenes, whereas the oxidation could be either reversible (diaza **3**) or irreversible (dioxa **1** and azaoxa **2**).

From the recorded voltammograms of **1**, **2**, and **3**, the corresponding fundamental gaps were estimated in a first approximation (Table 1).[15] For the irreversible oxidation waves, the peak potentials may shift depending on the scan rate, the concentration, and the kinetics of the subsequent chemical reactions. Even if the peak potential could not be considered as the standard potential for the oxidation of **1** and **2**, we used this value to estimate the fundamental gap and to compare the resulting values with those from the optical experiments. Taking into account this approximation, only a minor contribution of the N atom can be seen upon comparing dioxa **1** and azaoxa **2**. Diaza **3** stands apart, with a fundamental gap energy substantially lower than those of the other two carbocationic species. In an effort to gain more insights into the electronic properties of compounds **1**–**3**, we investigated their optical properties and determined their optical gaps.

Absorption and fluorescence

The electronic absorption and fluorescence properties of [6]helicenes **1**–**3** were recorded in acetonitrile (Figure 4 and Table 2). The absorption spectrum of diaza [6]helicene **3** shows an intense ($\varepsilon = 14\,700\ M^{-1}\,cm^{-1}$) lowest-energy transition centered at 614 nm, presenting a shoulder at higher energy, reminiscent of its parent diaza [4]helicene cation.[5a] Compounds **1** and **2** both exhibit a blueshifted absorption maximum at 562 nm. The absorption profiles and molar extinction coefficients are comparable for **1** and **3**, whereas noticeable broadening and a hypochromic shift of the absorption peak are highlighted for the azaoxa derivative **2** ($\varepsilon = 10\,700\ M^{-1}\,cm^{-1}$). Optical gaps of 2.15, 2.11, and 1.95 eV were determined for **1**, **2**, and **3**, respectively (Table 1). The difference in energy between the fundamental gap and the optical gap, that is, the electron–hole pair binding energy, is rather low for **1** (0.11 eV) compared with those for **2** and **3** (0.27 and 0.17 eV, respectively).[15b,16]

In terms of emission, helicene **3** displays a fluorescence covering the whole orange–red range with a maximal peak intensity at 658 nm. Dioxa **1** and azaoxa **2** present blueshifted emission maxima centered at 595 and 614 nm, respectively.

Table 2. Spectroscopic properties of **1**–**3** and substituted diaza[6]helicenes **4**–**15** in acetonitrile.

Cpd	Substituents: positions	λ_{abs} [nm]	ε [10^3 M^{-1} cm^{-1}]	λ_{em} [nm]	ϕ_{fl} [%]		τ [ns]	k_R [10^6 s^{-1}][a]	k_{NR} [10^6 s^{-1}][b]
1	–	562	15.5	595	12[c]	9[e]	4.0	30.0	220
2	–	562	10.7	614	22[c]	19[e]	6.8	32.3	115
3	–	614	14.7	658	31[c]	20[d]	9.8	31.6	70.4
4	NO_2: 8,10	560	18.2	591	46[c]	50[e]	10.9	42.2	49.5
5	Cl: 8,10	630	14.4	690	13[c]	8[d]	6.1	31.3	143
6	Br: 8,10	622	10.5	678	6.5[c]	4[d]	3.0	21.7	312
7	I: 8	620	13.4	675	2.6[c]	1.5[d]	1.0	26.0	974
8	Ph: 8,10	642	9.8	711	1.6[d]		2.0	8.0	492
9	*p*-anisyl: 8,10	657	8.9	755	<1[d]		0.3[f]	6.7	3330
10	PhC≡C: 8,10	650	8.3	740	<1[d]		0.6[f]	5.0	1660
11	NH_2: 8,10	731	1.9	–	–		–	–	–
12	NMe_2: 8,10	724	4.6	–	–		–	–	–
13	CN: 5,13	682	8.2	731	1.0[d]		0.7[f]	14.3	1410
14	NHPr: 5	582	22.9	619	70[c]		12.3	56.9	24.4
15	NHPr: 5, Br: 8,10	598	27.4	645	5.0[c]	5.0[d]	0.9[f]	55.6	1060

[a] $k_R = \phi/\tau$. [b] $k_{NR} = (1-\phi)/\tau$. [c] Relative to cresyl violet (MeOH, $\phi_{fl} = 54\%$). [d] Relative to oxazine 725 (EtOH, $\phi_{fl} = 11\%$). [e] Relative to sulforhodamine 101 (EtOH, $\phi_{fl} = 95\%$). [f] Fluorescence lifetimes measured by fluorescence upconversion technique. All the fluorescence decays were fitted as monoexponential functions. Lifetimes are given with an error of +/−0.1 ns for the TCSPC data and +/−0.3 ps for the upconversion data.

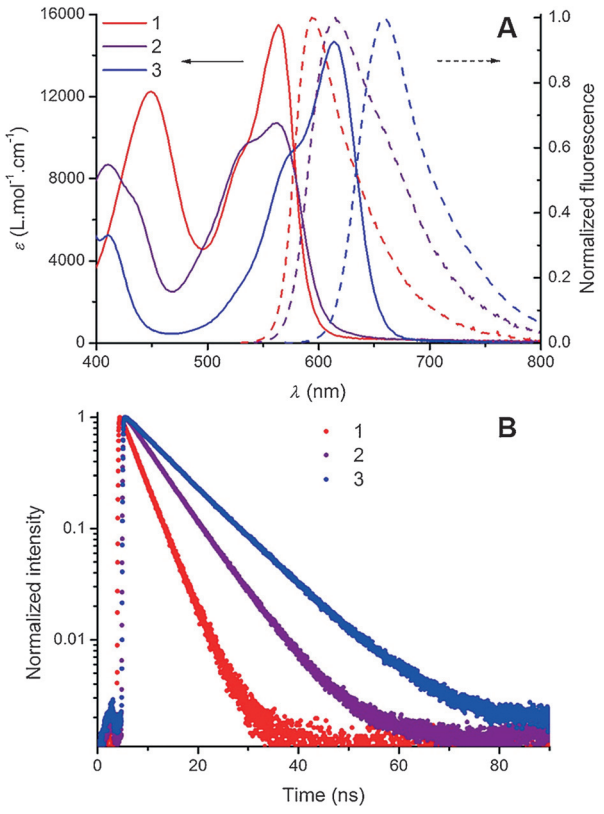

Figure 4. A) Absorption (plain lines) and normalized fluorescence spectra (dashed lines) of dioxa (**1**, red), azaoxa (**2**, purple), and diaza [6]helicene (**3**, blue) in acetonitrile (2.10^{-5} mol L^{-1}). B) Intensity normalized fluorescence time profiles.

Considering their luminescence located around or beyond 600 nm, **1**, **2**, and **3** possess relatively high fluorescence quantum yields of 12, 22, and 31%, respectively (with cresyl violet as reference, see Table 2). Note that the introduction of N atom(s) within the cationic scaffold causes a progressive red-shift in the emission band and enhances the fluorescence quantum yield. The corresponding lifetimes follow the same trend, with relatively high values of 4.0, 6.8, and 9.8 ns for **1**, **2**, and **3**, respectively. As shown in Table 2, the radiative rate constants calculated from the fluorescence quantum yields and lifetimes are essentially the same for **1**, **2**, and **3**, pointing to differences in internal conversion and/or intersystem-crossing efficiencies (vide infra). Interestingly, although **1** and **2** feature similar absorption maxima, their fluorescence spectra are not concomitant (excitation spectra are provided in Figures S9–S11, Supporting Information).

The influence of different solvents on the optical properties of **1**–**3** was also investigated (nine solvents, see Tables S1–S3 and Figures S12–S20, Supporting Information). Globally, the absorption and emission maxima of **1**–**3** exhibit only minor dependences on the selected solvent and the profiles, that is, the shape and intensity of the spectra did not change significantly. However a non-monotonic evolution of the optical properties is observed regarding the wide range of different polarities, refractive indexes, and viscosities of the solvents tested. Compounds **1**–**3** exhibit larger Stokes shifts in DMSO than in any other solvents (946, 1653, and 1069 cm^{-1} for **1**, **2**, and **3**, respectively). For **1**, it was found that the helicene degraded during the measurements in THF, methanol, and pentanol, which is unsurprising considering its lower chemical stability as indicated by the pK_{R+} value of 8.8 (vide supra). Note that **1**–**3** conserve a non-negligible fluorescence quantum yield in water (from 7% for **2** up to 10% for **3**), which is important for their possible use as red bioimaging probes.[5b,17]

Transient absorption and triplet quantum yields

Transient absorption measurements were performed in two temporal windows: 0–2 ns with 150 fs instrument response function[18] and 400 nm excitation (**2** and **3**, Figures S22 and S24, Supporting Information), and 0–100 μs with 350 ps instru-

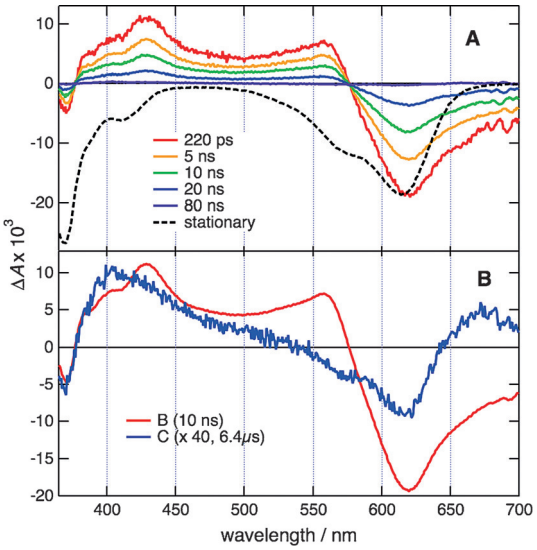

Figure 5. A) Transient absorption spectra measured at several time delays after 355 nm excitation of **3** in acetonitrile and inverted stationary absorption spectrum (dashed). B) Species-associated difference absorption spectra obtained from a global target analysis assuming a B→C→ scheme (A→B corresponding to the equilibration of the S_1 state occurs on the picosecond timescale (Figure S24, Supporting Information).

ment response function and 355 nm excitation (**1**–**3**, Figures 5, S21, and S23).[19] The early transient spectra exhibit both negative and positive bands. The negative bands coincide with the stationary electronic spectra, and thus, can be attributed to both the bleach of the ground-state absorption and the stimulated $S_1 \rightarrow S_0$ emission. The positive bands can be ascribed to $S_n \leftarrow S_1$ absorption.

Small spectral changes that are probably caused by the dissipation of the excess excitation energy can be observed during the first few picoseconds (Figures S22 and S24). Subsequently, the intensity of all spectral features decreases on the 5–10 ns timescale. This results in a spectrum with very small amplitude still containing the negative band owing to the bleach of ground-state absorption, and decaying on the microsecond timescale (Figures 5, S21, and S23). These transient spectra were analyzed globally assuming a series of successive exponential steps.[20] Three steps, that is, an A→B→C→ scheme, had to be used to reproduce the 0–2 ns and 0–100 μs data. The first one, associated with a picosecond time constant, can be ascribed to the equilibration of the lowest singlet excited state. The time constant of the B→C step coincides with the fluorescence lifetime measured by time-correlated single photon counting (TCSPC), and consequently, B can be interpreted as the S_1 state. Finally, as the C→D step occurs on the 10 μs timescale in N_2-bubbled solutions and is faster in the presence of air, species C is assigned to the triplet state. Through comparison of the relative amplitude of the bleach in the spectra associated with species B and C, the triplet yields of **1**–**3** can be estimated to be smaller than 5%. We therefore conclude that the main deactivation pathways of the S_1 state of **1**–**3** are fluorescence and internal conversion to the ground state.

Circularly polarized luminescence

As mentioned above, [6]helicenes **1**–**3** are chiral and can be isolated as single enantiomers through ion-pairing strategies (e.g., **3**) or, more generally, through Chiral Stationary Phase (CSP) HPLC resolution.[1,4] Strong chiroptical properties are recorded in the visible range of the light spectrum, as evidenced by the intense Cotton effects observed in the electronic circular dichroism spectra.[4] As such, it was deemed interesting to investigate their circularly polarized luminescence. The CPL spectra presented in Figure 6 were recorded in dichloromethane and show opposite signals for (+) versus (−) enantiomers of **1**–**3**.

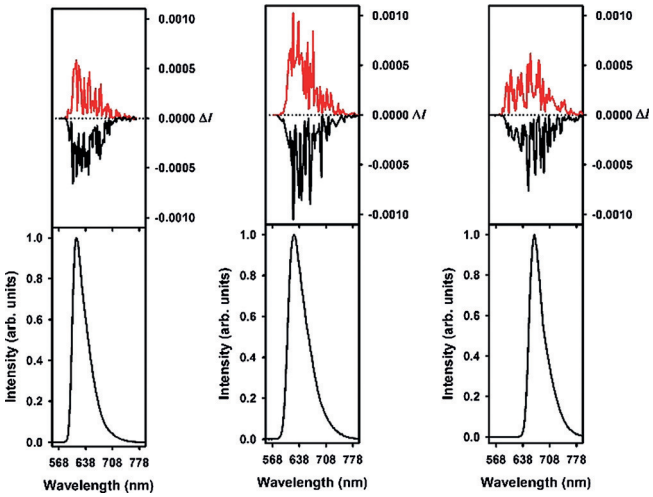

Figure 6. Circularly polarized luminescence (upper curve) and total luminescence (lower curve) spectra of (+) and (−)-**1** (left), -**2** (middle), and -**3** (right) in 2 mM degassed dichloromethane solutions at 295 K, upon excitation at 435/435, 442/435, and 473/472 nm, respectively (black for (+) and red for (−)).

The g_{lum} values are estimated to be −0.00032/+0.00041, −0.0021/+0.0020, and −0.0012/+0.0010 at the vicinity of the maximum emission wavelength for (+)- and (−)-**1**, **2**, and **3**, respectively (i.e., 595, 614, and 658 nm, respectively). These values are of the same order of magnitude as those for other examples of organic CPL-active helicenes.[5c,21] In a general fashion, the CPL properties are influenced only marginally by the replacement of O atom(s) by more electron-donating amino group(s) in **1** to **3**. This indicates that the chiral structures are more or less equivalent in terms of generating similar CPL activities, and the replacement did not affect the chiral properties at least from a CPL standpoint.

Tuning properties through chemical substitutions (4–15)

Absorption and fluorescence

Previously, the ability of cationic diaza [6]helicene **3** to react regioselectively with both electrophilic and nucleophilic reagents was evidenced.[1] Typically, in one step, substituents such as NO_2 (**4**), Cl (**5**), Br (**6**), and I (**7**) were introduced in positions 8

(and 10), and CN functional groups were added to positions 5 and 13 (helicene **13**). The dibromo derivative **6** was further engaged in Pd-catalyzed cross-coupling reactions, yielding bis(phenyl) **8** and bis(ethynyl) **10** helicenes. Reduction of dinitro **4** provided the corresponding bis(amino) **11**. Care was taken to prepare three new functionalized derivatives, namely bis(*p*-anisyl) **9**, bis(dimethylamino) **12**, and propylamino **14** (Figure 7).[22] The absorption and fluorescence properties of these compounds carrying electron-donating (EDG), electron-withdrawing (EWG), and possibly a combination of both types of groups were investigated. Selected spectra are presented in Figure 8 and the results are compiled in Table 2.

The influence of the substitution pattern in positions 8 and 10 was analyzed first (**4**–**12**). The presence of strong EWGs such as nitro moieties induces significant blueshifts of both the absorption and emission spectra of the whole series compared with **3**. Chromophore **4** possesses the lowest transition energy (560 nm, $\varepsilon = 18\,200\ \text{M}^{-1}\text{cm}^{-1}$) and is particularly fluorescent ($\phi_{fl} = 46\,\%$) at 591 nm. The effect of halogen atoms on the absorption properties is less pronounced: the lowest-energy absorption bands are slightly redshifted compared to **3** ($\Delta\lambda =$ 6–16 nm) in the order Cl > Br > I, and the extinction coefficients remain mostly unchanged, with the exception of the dibromo derivative **6** ($\varepsilon = 10\,500\ \text{M}^{-1}\text{cm}^{-1}$). However, in this series, going from **5** to **7**, a decrease in both the fluorescence quantum yields and lifetimes is observed, which is attributed to heavy atom effects (vide infra).[23] The introduction of phenyl or phenylethynyl moieties (**8** and **10**) induces a redshift of the absorption and emission bands, along with a decrease in the absorption molar extinction coefficient. The adjunction of electron-donating methoxy groups on the aryl substituents (**9**) further enhances this redshift for both absorption and emission. From the smaller k_R values of **8**–**10** and the larger Stokes shifts, it seems that the excited state has a substantial charge-transfer (CT) character, which increases upon going from **8** to **9** and **10**. In addition, an enhanced nonradiative de-excitation through the rotation of the aryl groups can be considered.

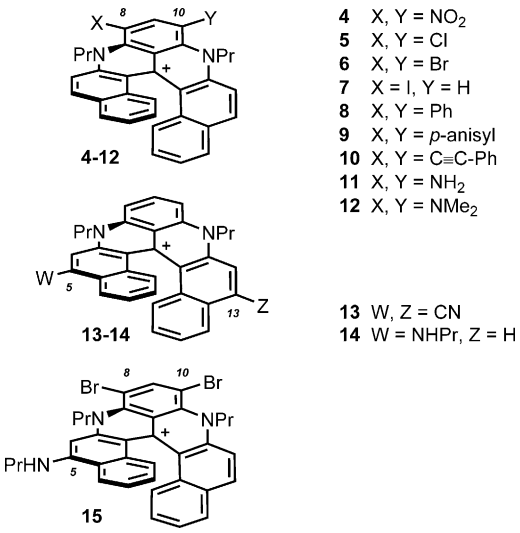

4 X, Y = NO_2
5 X, Y = Cl
6 X, Y = Br
7 X = I, Y = H
8 X, Y = Ph
9 X, Y = *p*-anisyl
10 X, Y = C≡C-Ph
11 X, Y = NH_2
12 X, Y = NMe_2

13 W, Z = CN
14 W = NHPr, Z = H

Figure 7. Substituted diaza [6]helicenes **4**–**15** carrying auxochrome substituents at positions 5, 8, 10, or 13. The BF_4^- counterion is omitted for clarity.

The introduction of a strong EDG in the amino (**11**) and dimethylamino (**12**) derivatives induces larger bathochromic and hypochromic shifts of the absorption spectra, along with broadening of the bands. However, these compounds are non-fluorescent, probably because of an intramolecular charge transfer along with a strong influence of the energy gap law, which quench the fluorescence (see computational study below).[23,24]

The effect of substitutions by EWGs and EDGs at positions 5 and/or 13 was also studied. The presence of EWGs in positions 5 and 13 induces a bathochromic shift of the optical properties. The bis(cyano) derivative **13** exhibits a lower-energy absorption band centered at 682 nm and weak fluorescence in the far-red ($\lambda_{em} = 731$ nm, with $\phi_{fl} < 1\,\%$). Alternatively, an EDG such as the amino NHPr group in position 5 leads to hypsochromic and hyperchromic shifts in absorption, with **14** absorbing at 582 nm ($\varepsilon = 22\,900\ \text{M}^{-1}\text{cm}^{-1}$) and emitting at 619 nm with a remarkable quantum efficiency of 70 %. To the best of our knowledge, this is the first time that such a strong fluorescence has been measured for an organic helicene in the orange–red region.[5] The reverse influence of EWGs and EDGs in positions 8 and 10 or 5 and 13 is notable. Whereas EWGs in positions 8 and 10 induce a blueshift of the optical properties, EDGs in the same positions lead to a redshift. The opposite trend is observed in positions 5 and 13. Finally, [6]helicene **15** was investigated; this compound bears both bromo EWG and

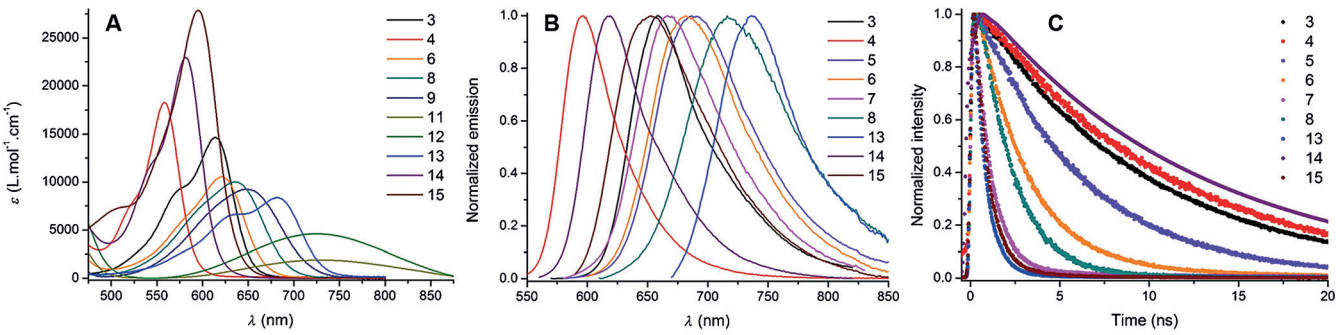

Figure 8. A) Selected absorption spectra, B) normalized fluorescence spectra, and C) normalized fluorescence decays of post-functionalized [6]helicenes in acetonitrile.

NHPr EDG substituents at positions 8, 10, and 5, respectively. Comparison with **14** clearly indicates a moderate influence of the bromine atoms in terms of absorption ($\lambda_{abs}=598$ vs. 582 nm, respectively), but a drastic lowering of the emission properties ($\phi_{fl}=5\%$ vs. 70%, respectively). The same trend is observed on comparison of unsubstituted **3** with dibromo **6**.

Transient absorption measurements in the 0–2 ns time window were performed with the iodo derivative **7** (Figure 9 A, B). The early spectra are dominated by a negative band at

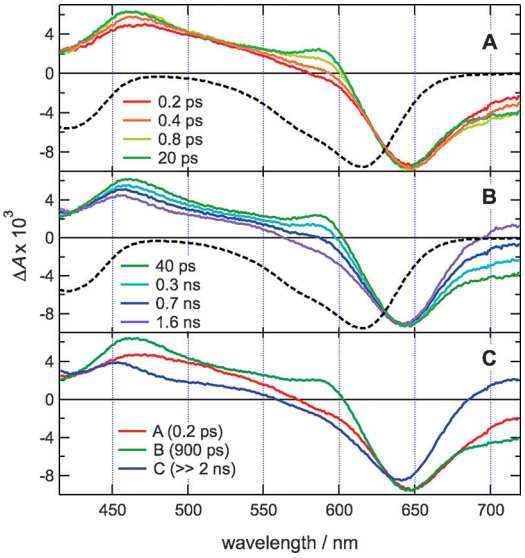

Figure 9. A, B) Transient absorption spectra recorded at various time delays after 400 nm excitation of **7** in acetonitrile and inverted stationary absorption spectrum (dashed). C) Species-associated difference absorption spectra obtained from a global target analysis assuming an A→B→C→ scheme.

650 nm and a positive band peaking at 460 nm. The negative band is caused by the bleach of the ground-state absorption and its red edge to stimulated emission. The positive band can be assigned to $S_n \leftarrow S_1$ absorption. The negative band is red-shifted relative to the $S_1 \leftarrow S_0$ band, suggesting partial overlap of the excited-state absorption. During the first picosecond, the positive band changes its shape and acquires a shoulder at around 600 nm, and the red side of the negative band increases. Given the substantial amount of excess excitation energy, these effects can be assigned to the equilibration of the S_1 state. Subsequently, the transient spectra remain essentially unchanged up to about 100 ps, and then evolve on a timescale of hundreds of picoseconds into a long-lived spectrum in which the 600 nm shoulder and the stimulated emission are absent. These data could be reproduced assuming an A→B→C scheme with the first and second steps associated with a 0.2 and 900 ps time constant, respectively (Figure 9 C). The short time constant agrees with the equilibration of the S_1 state, whereas the second one is similar to the fluorescence lifetime. Given the small fluorescence quantum yield of **7** and the presence of the iodine substituent, the long-lived transient C is interpreted as the triplet state. As the absorption of both the S_1 and T_1 states overlaps partially with the bleach, precise determination of the triplet quantum yield from the relative intensity of the bleach in the spectra associated with species B and C is difficult. However, assuming similar absorptions of both S_1 and T_1 states in the overlapping region, the triplet quantum yield can be estimated to be on the order of 80–90%.

Rationalization through computational analysis

To obtain further insights into the nature of the electronic excited states, we performed first-principles calculations. These relied on a hybrid CC2/TD-DFT protocol that allows reliable 0–0 energies to be obtained.[25] These energies can be compared directly to the crossing point between the absorption and emission spectra.[26] The results of this theoretical investigation are listed in Table 3. The agreement between the CC2/TD-DFT values and experimental results is very satisfying, with an average absolute deviation as small as 12 nm. The uncorrected TD-DFT approach nicely restores the auxochromic trends but delivers too small wavelengths. Experimentally, both **11** and **12** were found to be nonfluorescent, which can be understood from the calculations. Indeed, the computed CC2 emission energies for these two compounds are 1416 and 1446 nm, indicating a very strong structural relaxation of the excited state. Such wavelengths correspond to a gap lower than 1 eV, which is clearly not favorable for the emission according to the energy gap law.

Table 3. Comparison between experimental and theoretical 0–0 energies for the treated dyes. Note that during the theoretical calculations the alkyl chains were substituted by methyl groups. All values are in nm.

Cpd	Exptl	Theory (CC2/TD-DFT)	Theory (TD-DFT)
1	578	574	493
2	589	592	507
3	635	634	535
4	577	569	490
11[a]	731	738	634
12[a]	724	748	610
13	708	730	600
14	599	595	513

[a] Experimental λ_{max} and theoretical vertical absorption.

Experimentally, it was found that a strong EWG induces hypsochromic/bathochromic shifts if located at positions 8,10/5,13, whereas EDGs yield the opposite trend. As TD-DFT revealed that the lowest-energy transitions present a strongly dominant HOMO–LUMO contribution, we plotted these orbitals for compound **3** (Figure 10). The HOMO presents significant density at positions 8 and 10, meaning that the addition of an EWG (EDG) stabilizes (destabilizes) its energy and hence increases (decreases) the gap as the LUMO is almost unaffected. In contrast, the LUMO displays significant contributions at positions 5 and 13, so that the addition of an EWG (EDG) stabilizes (destabilizes) its energy and hence decreases (increases) the gap. Therefore, by playing with these positions, one can tune (almost) independently the levels of the two frontier orbitals. This fits perfectly with the measured evolutions.

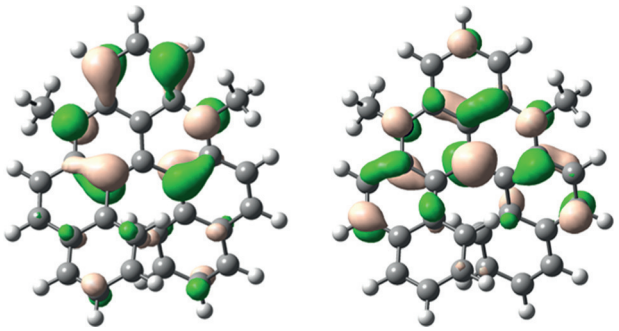

Figure 10. HOMO (left) and LUMO (right) of **3**.

The computed and convoluted absorption lineshapes are represented in Figure 11 for compounds **1**–**3**. As in the experimental spectra, **1** does not exhibit a clear-cut broadening feature, whereas both **2** and **3** present a shoulder. Interestingly, the relative intensities for **1** and **3** are highly similar, whereas the intensity of **2** is 24% lower, as also observed in the experimental data (decrease in the extinction coefficient of 27%).

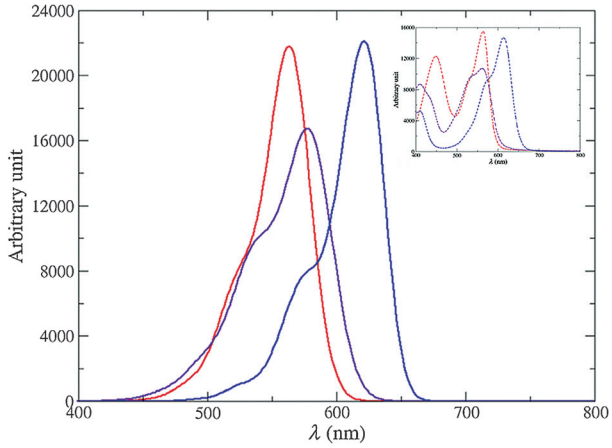

Figure 11. Computed vibronic absorption spectra of **1** (red), **2** (purple), and **3** (blue). For their convolution, a HWHM of 0.06 eV was employed for **1** and **2**, and 0.04 eV for **3**. The inset represents the experimental data.

To gain further insights into the origins of specific band shapes, we identified the key vibronic contributions for the three dyes. Figure S25 (Supporting Information) shows the normalized experimental and theoretical absorption and fluorescence lineshapes together with the *stick* vibronic contributions. Overall, a good agreement between theory and experiment is observed for both positions and bandshapes. Nevertheless, the positions of the maximum bands in the absorption spectra are redshifted for **2** and **3** but slightly blueshifted for **1**. The computed fluorescence spectra are systematically blueshifted. We observe a significant difference in bandshapes caused by the substitution of oxygen by N–CH_3. Table S4 and Figure S26 (Supporting Information) list the key vibrational modes, explaining band broadening and the presence of shoulders. In **1**, the maximum band involves, beyond the 0–0 transition, three intense vibronic couplings related to the low-frequency vibrations of the naphthalene subunits with scissoring/bending (mode 3) and distortions involving C–C twisting and rocking vibrations (modes 8 and 11). In addition, the small shoulder observed in the spectra arises mainly from the contribution of the high-frequency C–C asymmetric stretching (breathing) mode of the entire structure (mode 91 in Table S4). Replacing one oxygen atom by a N–CH_3 moiety modifies the vibronic contributions of the main band owing to the introduction of a certain asymmetry of the molecule inducing three vibronic contributions with equivalent intensities (0.34). Each of these modes includes the rocking of the naphthalene located on the N–CH_3-substituted ring [Na(N)] with the rest of the conjugated molecules undergoing a wagging (mode 1) or a twisting (modes 5 and 14) vibration. Similarly to **1**, a high-frequency mode corresponding to the breathing of the structure is responsible for the shoulder. The vibronic modes of **3** are highly similar to those of **2**; more particularly, modes 1, 5, 40, and 105 of **3** correspond to modes 1, 5, 14, and 98 of **2** (see Supporting Information). Nevertheless, two supplementary modes appear, that is, the CH_3 rotation (mode 12) and the asymmetric C–C stretching of the conjugated moiety between the N–CH_3 substituted rings (mode 119). Modes 105 and 119 combine to give the shoulder.

Conclusions

The chemical stabilities and electrochemical and optical properties of a series of cationic hetero [6]helicenes have been studied to reveal a drastic influence of 1) the heteroatoms within the helical core and 2) auxochrome substituents introduced at the periphery. An increasing chemical stability is evidenced for cationic dioxa **1**, azaoxa **2**, and diaza **3** [6]helicenes through the measurement of (large) pK_{R+} values of 8.8, 15.2, and 20.4, respectively. Clearly, the replacement of the O atom(s) by more electron-donating amino group(s) going from dioxa (**1**) to diaza (**3**) is beneficial for the chemical stability. The same trend is observed through electrochemistry: the reduction and oxidation potentials of the cations are lowered substantially from **1** to **3** (i.e., from −0.12 to −0.72 V for $E^{red}_{1/2}$). In terms of optical properties, the influence of the substitution of internal atom(s) (O→N) is again prominent, inducing a bathochromic shift in absorption and emission on going from **1** to **3**. Interestingly, both quantum yields (12, 22, and 31% for **1**, **2**, and **3**, respectively) and fluorescence lifetimes (4.0, 6.8, and 9.8 ns for **1**, **2**, and **3**, respectively) increase in this order. Moreover, those fluorophores exhibit only marginal solvatochromism (absorption and emission). Transient absorption measurements indicate that the first singlet excited states of **1**, **2**, and **3** decay mostly through fluorescence and internal conversion to the ground state, intersystem crossing being much less efficient, with a triplet quantum yield smaller than 5%. However, upon substitution with a heavy atom such as iodine, intersystem crossing to the triplet state becomes the dominant decay pathway. Isolated as single enantiomers, **1**–**3** emit circularly polarized light, the most efficient CPL emitter being the nonsymmetrical azaoxa **2** (g_{lum} −0.0021/+0.0020). Further tuning of

the electronic properties was achieved through the addition of electron-donating or electron-withdrawing substituents at the periphery of **3**. Highly efficient luminophores (ϕ_{fl} up to 70%) or far-red absorbers (λ_{max} up to 730 nm) are now accessible. Interestingly, the influence of EWGs in positions 8 and 10 is opposite to that in positions 5 and 13 (blueshift vs. redshift), and vice versa for EDGs. This was rationalized through computational studies, which revealed significant differences in the topology of the frontier orbitals. Applications in several fields of chemistry can be foreseen, from bioimaging to polarized emitting devices.[17,27]

Acknowledgements

We thank the University of Geneva, the Swiss National Science Foundation, and the NCCR chemical biology funded by the Swiss National Science Foundation. We also acknowledge the contributions of the Sciences Mass Spectrometry (SMS) platform at the Faculty of Sciences, University of Geneva. H.L. acknowledges the China Scholarship Council for his PhD fellowship. D.J. acknowledges the European Research Council (ERC) and the Région des Pays de la Loire for financial support in the framework of a starting grant (Marches-278845) and the LumoMat project, respectively. This research used the resources of: 1) the GENCI-CINES/IDRIS, 2) CCIPL (Centre de Calcul Intensif des Pays de Loire), and 3) a local Troy cluster. G.M. thanks the NIH, Minority Biomedical Research Support (grant 1 SC3 GM089589-07) and the Henry Dreyfus Teacher–Scholar Award for financial support, and R.C.T. thanks the SJSU RISE program (NIH grant 5R25M71381) for a research fellowship.

Keywords: circularly polarized luminescence · density functional calculations · electrochemistry · fluorescence · helicenes

[1] F. Torricelli, J. Bosson, C. Besnard, M. Chekini, T. Bürgi, J. Lacour, *Angew. Chem. Int. Ed.* **2013**, *52*, 1796 – 1800; *Angew. Chem.* **2013**, *125*, 1840 – 1844.

[2] a) Y. Shen, C.-F. Chen, *Chem. Rev.* **2011**, *111*, 1463 – 1535; b) M. Gingras, *Chem. Soc. Rev.* **2013**, *42*, 968 – 1006; c) M. Gingras, G. Felix, R. Peresutti, *Chem. Soc. Rev.* **2013**, *42*, 1007 – 1050; d) M. Gingras, *Chem. Soc. Rev.* **2013**, *42*, 1051 – 1095; e) A. Urbano, *Angew. Chem. Int. Ed.* **2003**, *42*, 3986 – 3989; *Angew. Chem.* **2003**, *115*, 4116 – 4119; f) N. Hoffmann, *J. Photochem. Photobiol. C* **2014**, *19*, 1 – 19; g) A. Rajca, M. Miyasaka, in *Functional Organic Materials* (Eds.: T. J. J. Müller, U. H. F. Bunz), Wiley-VCH, Weinheim, **2007**, pp. 543 – 577; h) I. G. Stará, I. Starý, in *Science of Synthesis Vol. 45* (Eds.: J. S. Siegel, Y. Tobe), Thieme, Stuttgart, **2010**, pp. 885 – 953; i) F. Dumitrascu, D. G. Dumitrascu, I. Aaron, *ARKIVOC (Gainesville, FL, U.S.)* **2010**, 1 – 32; j) M. J. Narcis, N. Takenaka, *Eur. J. Org. Chem.* **2014**, 21 – 34; k) J. Bosson, J. Gouin, J. Lacour, *Chem. Soc. Rev.* **2014**, *43*, 2824 – 2840.

[3] Throughout this report, the BF_4^- anionic counterions that are present to balance the positive charges are omitted for reasons of clarity. The influence of the side chains is not investigated.

[4] G. M. Labrador, J. Bosson, Z. S. Breitbach, Y. Lim, E. R. Francotte, R. Sabia, C. Villani, D. W. Armstrong, J. Lacour, *Chirality* **2016**, *28*, 282 – 289.

[5] a) O. Kel, P. Sherin, N. Mehanna, B. Laleu, J. Lacour, E. Vauthey, *Photochem. Photobiol. Sci.* **2012**, *11*, 623 – 631; b) M. Li, Y. Niu, X. Zhu, Q. Peng, H.-Y. Lu, A. Xia, C.-F. Chen, *Chem. Commun.* **2014**, *50*, 2993 – 2995; c) Y. Sawada, S. Furumi, A. Takai, M. Takeuchi, K. Noguchi, K. Tanaka, *J. Am. Chem. Soc.* **2012**, *134*, 4080 – 4083; d) H. Sakai, S. Shinto, Y. Araki, T. Wada, T. Sakanoue, T. Takenobu, T. Hasobe, *Chem. Eur. J.* **2014**, *20*, 10099 – 10109; e) H. Oyama, K. Nakano, T. Harada, R. Kuroda, M. Naito, K. Nobusawa, K. Nozaki, *Org. Lett.* **2013**, *15*, 2104 – 2107; f) T. Matsuno, Y. Koyama, S. Hiroto, J. Kumar, T. Kawai, H. Shinokubo, *Chem. Commun.* **2015**, *51*, 4607 – 4610; g) I. H. Delgado, S. Pascal, A. Wallabregue, R. Duwald, C. Besnard, L. Guenee, C. Nancoz, E. Vauthey, R. C. Tovar, J. L. Lunkley, G. Muller, J. Lacour, *Chem. Sci.* **2016**, *7*, 4685 – 4693.

[6] a) V. Nair, S. Thomas, S. C. Mathew, K. G. Abhilash, *Tetrahedron* **2006**, *62*, 6731 – 6747; b) D. F. Duxbury, *Chem. Rev.* **1993**, *93*, 381 – 433.

[7] This type of reactivity with NaOH corresponds to a nucleophilic attack rather than a Brønsted acid/base reaction as observed with azahelicenes, for instance. See J. Vacek Chocholoušová, J. Vacek, A. Andronova, J. Míšek, O. Songis, M. Šámal, I. G. Stará, M. Meyer, M. Bourdillon, L. PospíŠil, I. Starý, *Chem. Eur. J.* **2014**, *20*, 877 – 893.

[8] B. W. Laursen, F. C. Krebs, *Chem. Eur. J.* **2001**, *7*, 1773 – 1783.

[9] B. W. Laursen, F. C. Krebs, *Angew. Chem. Int. Ed.* **2000**, *39*, 3432 – 3434; *Angew. Chem.* **2000**, *112*, 3574 – 3576.

[10] For **1**, **2**, and **3**, the R^2 coefficients of determination are 0.9925, 0.9989, and 0.9891, respectively. Upon immediate acidification after measurements, the absorption spectra of the carbenium species are recovered.

[11] The slope of the trendlines being different from unity, competitive reactions could not be ruled out. See the Supporting Information.

[12] a) C. Herse, D. Bas, F. C. Krebs, T. Buergi, J. Weber, T. Wesolowski, B. W. Laursen, J. Lacour, *Angew. Chem. Int. Ed.* **2003**, *42*, 3162 – 3166; *Angew. Chem.* **2003**, *115*, 3270 – 3274; b) T. J. Sørensen, M. F. Nielsen, B. W. Laursen, *ChemPlusChem* **2014**, *79*, 1030 – 1035; c) T. J. Sørensen, A. Ø. Madsen, B. W. Laursen, *Chem. Eur. J.* **2014**, *20*, 6391 – 6400; d) J. Gouin, T. Bürgi, L. Guénée, J. Lacour, *Org. Lett.* **2014**, *16*, 3800 – 3803; e) J. Guin, C. Besnard, J. Lacour, *Org. Lett.* **2010**, *12*, 1748 – 1751; f) T. J. Sørensen, A. Ø. Madsen, B. W. Laursen, *Tetrahedron Lett.* **2013**, *54*, 587 – 590.

[13] Repetitive cleaning and polishing of the electrode surface is mandatory to record accurate and reproducible CVs as these compounds have a strong tendency to adsorb at the surface of the working electrode.

[14] C. Adam, A. Wallabregue, H. Li, J. Gouin, R. Vanel, S. Grass, J. Bosson, L. Bouffier, J. Lacour, N. Sojic, *Chem. Eur. J.* **2015**, *21*, 19243 – 19249.

[15] a) S. Janietz, D. D. C. Bradley, M. Grell, C. Giebeler, M. Inbasekaran, E. P. Woo, *Appl. Phys. Lett.* **1998**, *73*, 2453 – 2455; b) J.-L. Bredas, *Mater. Horiz.* **2014**, *1*, 17 – 19.

[16] As already mentioned, the oxidation process is almost completely irreversible for **1** and **2** and the calculated fundamental gaps are just approximated values for these two compounds. However, the trend observed with the lower values calculated from the CV curves for **3** in comparison to **1** and **2** correlates with the optical gap (Table 1). Thus, it validates the approximation used for the calculation of the fundamental gap.

[17] O. Kel, A. Fürstenberg, N. Mehanna, C. Nicolas, B. Laleu, M. Hammarson, B. Albinsson, J. Lacour, E. Vauthey, *Chem. Eur. J.* **2013**, *19*, 7173 – 7180.

[18] N. Banerji, G. Duvanel, A. Perez-Velasco, S. Maity, N. Sakai, S. Matile, E. Vauthey, *J. Phys. Chem. A* **2009**, *113*, 8202 – 8212.

[19] B. Lang, S. Mosquera-Vázquez, D. Lovy, P. Sherin, V. Markovic, E. Vauthey, *Rev. Sci. Instrum.* **2013**, *84*, 073107.

[20] I. H. M. van Stokkum, D. S. Larsen, R. van Grondelle, *Biochim. Biophys. Acta Bioenerg.* **2004**, *1657*, 82 – 104.

[21] a) K. E. S. Phillips, T. J. Katz, S. Jockusch, A. J. Lovinger, N. J. Turro, *J. Am. Chem. Soc.* **2001**, *123*, 11899 – 11907; b) J. E. Field, G. Muller, J. P. Riehl, D. Venkataraman, *J. Am. Chem. Soc.* **2003**, *125*, 11808 – 11809; c) R. Hassey, E. J. Swain, N. I. Hammer, D. Venkataraman, M. D. Barnes, *Science* **2006**, *314*, 1437 – 1439; d) T. Kaseyama, S. Furumi, X. Zhang, K. Tanaka, M. Takeuchi, *Angew. Chem. Int. Ed.* **2011**, *50*, 3684 – 3687; *Angew. Chem.* **2011**, *123*, 3768 – 3771; e) K. Nakamura, S. Furumi, M. Takeuchi, T. Shibuya, K. Tanaka, *J. Am. Chem. Soc.* **2014**, *136*, 5555 – 5558; f) C. Shen, E. Anger, M. Srebro, N. Vanthuyne, K. K. Deol, T. D. Jefferson, G. Muller, J. A. G. Williams, L. Toupet, C. Roussel, J. Autschbach, R. Reau, J. Crassous, *Chem. Sci.* **2014**, *5*, 1915 – 1927; g) N. Saleh, B. Moore, M. Srebro, N. Vanthuyne, L. Toupet, J. A. G. Williams, C. Roussel, K. K. Deol, G. Muller, J. Autschbach, J. Crassous, *Chem. Eur. J.* **2015**, *21*, 1673 – 1681; h) N. Saleh, M. Srebro, T. Reynaldo, N. Vanthuyne, L. Toupet, V. Y. Chang, G. Muller, J. A. G. Williams, C. Roussel, J. Autschbach, J. Crassous, *Chem. Commun.* **2015**, *51*, 3754 – 3757; i) S. Pascal, C. Besnard, F. Zinna, L. Di Bari, B. Le Guennic, D. Jacquemin, J. Lacour, *Org. Biomol. Chem.* **2016**, *14*, 4590 – 4594.

[22] See Schemes S1–S6 and details in the Supporting Information.
[23] B. Valeur, in *Molecular Fluorescence*, Wiley-VCH, Weinheim, **2001**, pp. 34 – 71.
[24] R. Englman, J. Jortner, *Mol. Phys.* **1970**, *18*, 145 – 164.
[25] D. Jacquemin, I. Duchemin, X. Blase, *J. Chem. Theory Comput.* **2015**, *11*, 5340 – 5359.
[26] a) D. Jacquemin, A. Planchat, C. Adamo, B. Mennucci, *J. Chem. Theory Comput.* **2012**, *8*, 2359 – 2372; b) L. Goerigk, S. Grimme, *J. Chem. Phys.* **2010**, *132*, 184103.
[27] a) M. T. Reetz, S. Sostmann, *Tetrahedron* **2001**, *57*, 2515 – 2520; b) S. Honzawa, H. Okubo, S. Anzai, M. Yamaguchi, K. Tsumoto, I. Kumagai, *Bioorg. Med. Chem.* **2002**, *10*, 3213 – 3218; c) Y. Xu, Y. X. Zhang, H. Sugiyama, T. Umano, H. Osuga, K. Tanaka, *J. Am. Chem. Soc.* **2004**, *126*, 6566 – 6567; d) R. Passeri, G. Gaetano Aloisi, F. Elisei, L. Latterini, T. Caronna, F. Fontana, I. Natali Sora, *Photochem. Photobiol. Sci.* **2009**, *8*, 1574 – 1582; e) L. Latterini, E. Galletti, R. Passeri, A. Barbafina, L. Urbanelli, C. Emiliani, F. Elisei, F. Fontana, A. Mele, T. Caronna, *J. Photochem. Photobiol. A* **2011**, *222*, 307 – 313; f) A. Rajapakse, K. S. Gates, *J. Org. Chem.* **2012**, *77*, 3531 – 3537; g) Y. Hu, B. Wex, M. W. Perkovic, D. C. Neckers, *Tetrahedron* **2008**, *64*, 2251 – 2258; h) L. Shi, Z. Liu, G. Dong, L. Duan, Y. Qiu, J. Jia, W. Guo, D. Zhao, D. Cui, X. Tao, *Chem. Eur. J.* **2012**, *18*, 8092 – 8099; i) P. E. Reyes-Gutiérrez, M. Jirasek, L. Severa, P. Novotna, D. Koval, P. Sazelova, J. Vavra, A. Meyer, I. Cisarova, D. Saman, R. Pohl, P. Stepanek, P. Slavicek, B. J. Coe, M. Hajek, V. Kasicka, M. Urbanova, F. Teply, *Chem. Commun.* **2015**, *51*, 1583 – 1586; j) A. Wallabregue, P. Sherin, J. Guin, C. Besnard, E. Vauthey, J. Lacour, *Eur. J. Org. Chem.* **2014**, 6431 – 6438.

Received: July 28, 2016
Published online on November 25, 2016